Terra Nova

Three-dimensional vorticity and time-constrained evolution of the Main Central Thrust zone, Garhwal Himalaya (NW India)

Journal:	*Terra Nova*
Manuscript ID	TER-2019-0086
Wiley - Manuscript type:	Paper
Date Submitted by the Author:	10-Sep-2019
Complete List of Authors:	Montemagni, Chiara; Università degli Studi di Milano-Bicocca, Dipartimento di Scienze dell'Ambiente e della Terra Carosi, Rodolfo; Università degli Studi di Torino, Dipartimento di Scienze della Terra Fusi, Nicoletta; Università degli Studi di Milano-Bicocca, Dipartimento di Scienze dell'Ambiente e della Terra Iaccarino, Salvatore; Università degli Studi di Torino, Dipartimento di Scienze della Terra Montomoli, Chiara; Università degli Studi di Torino, Dipartimento di Scienze della Terra Villa, Igor; Universitat Bern, Institut für Geologie Zanchetta, Stefano; Università degli Studi di Milano-Bicocca, Dipartimento di Scienze dell'Ambiente e della Terra
Keywords:	Shear zone, Kinematic vorticity RGN method, 3D microCT, Himalayan Main Central Thrust zone, ⁴⁰Ar/³⁹Ar geochronology

Three-dimensional vorticity and time-constrained evolution of the Main Central Thrust zone, Garhwal Himalaya (NW India)

Chiara Montemagni[1,*], Rodolfo Carosi[2], Nicoletta Fusi[1], Salvatore Iaccarino[2], Chiara Montomoli[2], Igor M. Villa[1,3] and Stefano Zanchetta[1]

1 Dipartimento di Scienze dell'Ambiente e della Terra, Università degli Studi di Milano – Bicocca

2 Dipartimento di Scienze della Terra, Università degli Studi di Torino

3 Institut für Geologie, Universität Bern

* Corresponding author: c.montemagni@campus.unimib.it

Abstract

Vorticity estimates based on porphyroclasts analysis is limited by the extrapolation to three dimensions of two-dimensional data. We describe a 3D approach based on the use of X-ray micro-computed tomography that better reflects the real geometry of the porphyroclasts population. The 3D kinematic vorticity analysis of the Munsiari Thrust mylonites, the lower boundary of the Main Central Thrust zone (MCTz) in Indian Himalaya, indicates a large pure shear component during non-coaxial shearing.

$^{40}Ar/^{39}Ar$ ages of micas along the mylonitic foliation of the Munsiari and Vaikrita thrusts (the upper boundary of the MCTz) constrain thrust activity to 5-4 and 8-9 Ma, respectively. Available kinematic vorticity analyses of the Vaikrita mylonites suggest the dominance of a simple shear component. Combining these data, we suggest that the southward and structurally downward shift of deformation

along the MCTz was accompanied by a progressive increase of the pure shear component in a general shear flow.

Keywords:

Shear zone, Kinematic vorticity RGN method, 3D microCT, Himalayan Main Central Thrust zone, $^{40}Ar/^{39}Ar$ geochronology.

1. Introduction

The Himalaya is commonly regarded as a cylindrical belt from west to east due to the impressive lateral continuity of the main litho-tectonic units and faults/shear zones, which is a peculiar feature of this mountain range. Nevertheless, along-strike differences in geological structures, topography, convergence rates and geochronology have been described in the literature (Hodges, 2000; Robert *et al*., 2011). The occurrence of regional shear zones makes the Himalaya the right place to investigate large-scale tectonics, kinematics and ages of these structures. The exhumation of the metamorphic core of the belt (the Greater Himalayan Sequence, GHS) was favored by the Main Central Thrust Zone (MCTz) at the bottom and the South Tibetan Detachment System (STDS; Caby *et al*., 1983; Burg *et al*., 1984) at the top of the GHS (Hodges *et al*. 1996). All along the orogenic belt, regional scale thrusts or shear zones accommodated crustal shortening related to the India-Eurasia convergence since the Middle-Late Eocene. These thrusts propagated in time and space towards the foreland, mostly or exclusively in-sequence (Montomoli *et al*., 2013; Carosi *et al*., 2016). The most prominent of these tectonic discontinuities is the MCTz (Heim and Gansser, 1939; Searle *et al*., 2008), a km-thick zone of intensively sheared rocks (Fig. 1), which separates the GHS from the underlying Lesser Himalayan Sequence (LHS), the latter consisting of low- to medium-grade metamorphic rocks (Arita, 1983). The exact localization of the MCTz boundaries together with its temporal and structural evolution are still a matter of debate (Searle *et al*., 2008; Martin, 2017; Carosi *et al*., 2018 for updated reviews). The time of activity of the MCTz ranges from 23-15 Ma up to c. 3 Ma in different areas of the belt (Godin *et al*., 2006; Montomoli *et al*., 2015). Such a long-lasting activity resulted in a complex structural and kinematic evolution, with the superposition of several deformation stages whose related structures are unevenly preserved along the thrust zone.

In the Garhwal Himalaya (NW India), the MCTz is bounded by two discrete fault zones, the Munsiari Thrust at the bottom and the Vaikrita Thrust at the top (Valdiya, 1980; Jain *et al*., 2014). According to Metcalfe (1993), the deformation towards the structurally upper part of the MCTz is completely ductile, whereas near the Munsiari Thrust fabrics related to ductile-brittle transition are observed. Within the MCTz the metamorphic grade increases structurally upward from the Munsiari Thrust to the Vaikrita Thrust, increasing in temperature from greenschist to amphibolite facies conditions (Metcalfe, 1993; Searle *et al*., 1993; Spencer *et al*., 2012; Jain *et al*., 2014; Thakur *et al*., 2015). The mylonitic foliation is associated to kinematic indicators that indicate a top-to-the-south movement in a flow regime apparently dominated by simple shear flow (Metcalfe, 1993).

The aim of this paper is to constrain age and kinematics of the upper and lower boundaries, the Munsiari and Vaikrita Thrust respectively, of the MCTz in the Garhwal Himalaya (Bhagirathi valley, NW India). The kinematic analysis has been performed with a new three-dimensional approach, described below, which improves the reliability of kinematic vorticity numbers estimated using the stable porphyroclasts method (Jessup *et al*., 2007).

2. Ages of mylonitic foliation along the Munsiari and Vaikrita Thrusts

Two mylonitic orthogneiss from the Munsiari Thrust (UT15-5; UT15-6) and one mylonitic micaschist from the Vaikrita Thrust (UT15-10) from the Bhagirathi valley, and one mylonitic calcschist from the Munsiari Thrust (AK18-13) in the Alaknanda valley (Fig. 1b-c), have been selected for $^{40}Ar/^{39}Ar$ dating (following the protocols of Bosio *et al*., 2019). A well-developed mylonitic foliation is observed in the selected samples; no evidence of brittle deformation was found.

Sample UT15-5 (Fig. 2a-b) contains quartz, K-feldspar, biotite, rare muscovite, monazite, allanite and zircon. The mylonitic foliation (S2 following Metcalfe, 1993) is defined by the shape preferred orientation (SPO) of micas, and can be defined as a disjunctive schistosity due to the alternation of granoblastic quartz-feldspathic layers and lepidoblastic ones. UT15-6 (Fig. 2c-d) contains quartz, K-feldspar, biotite, rare muscovite, titanite and zircon. As in the companion sample UT15-5, the SCC' fabric is ubiquitous and the mylonitic foliation (S2) is defined by the SPO of biotite. In both samples, we separated biotite for dating. As shown by Fig. 2, the different mica generations are intergrown at a scale < 10 μm.

AK18-13 consists of quartz, calcite, muscovite and biotite (Fig. 2e-f). The S2 is a disjunctive mylonitic foliation locally crenulated by a successive deformation. Sporadic S1 relict domains and late static micas occur (Fig. 2e).

Sample UT15-10 (Fig. 2g-h) contains muscovite, quartz, K-feldspar, garnet and post-mylonitic late chlorite. Ilmenite also grew along the main foliation. The S2 is an anastomosing crenulation cleavage, in which both the cleavage and pre-S2 microlithon domains are mica rich. S1 domains are ubiquitous, but have been almost totally overprinted by polygonal arcs (Fig. 2h; Passchier and Trouw, 2005), which predominate over the S1. Large crystals of post-S2 static muscovite also occur. In samples UT15-10 and AK18-13 we separated muscovite for $^{40}Ar/^{39}Ar$ dating. Dated mica separates were prepared by microdrilling the mylonitic foliation domains, crushing of the drilled cores, magnetic separation of micas and final hand picking. The age of biotite growth along the mylonitic foliation of the Munsiari Thrust in the Bhagirathi valley has been constrained at 4.81 ± 0.02 Ma and 4.78 ± 0.02 Ma for UT15-5 and UT15-6 respectively, whereas in the Alaknanda valley the S2 muscovite from the Munsiari Thrust gives 5.4 ± 0.02 Ma. For the Vaikrita Thrust we dated both syn-kinematic and post-kinematic muscovite of sample UT15-10 obtaining ages of 8.17 ± 0.06 Ma and 7.44 ± 0.12 Ma, respectively (Fig. 3, see Table 1 SUPP for $^{40}Ar/^{39}Ar$ data). The latter age likely represents the final phases of post-kinematic muscovite growth on the main foliation that follow the structurally downward propagation of the deformation. The argument that M2 biotites date the formation of the main foliation, and not some later cooling, is discussed in greater detail by Montemagni et al. (2019), who observed that if three coexisting mica generations give three different ages, then at least two of them must be formation ages. This applies to the Vaikrita Thrust, and a fortiori to the Munsiari Thrust, whose peak temperature was c. 100 °C lower.

3. Three-dimensional vorticity analysis

The theory of the stable porphyroclasts method relies on the fact that in a general shear flow porphyroclasts are partitioned into two populations. One rotates continuously and therefore does not develop a preferred orientation, the other aligns along a minimum energy position ("stable sink" position of Jessup *et al.*, 2007). The stable orientation analysis has yielded vorticity estimates (Xypolias, 2010 and references therein) to deduce large-scale tectonics of shear zones (Li and Jiang, 2011 and references therein) from different tectonic settings (Xypolias, 2010; Fossen and Cavalcante, 2017). However, severe limitations arise because a complex three-dimensional problem, the motion of rigid clasts, is reduced to its two-dimensional section or projection in the plane of the thin section (Iacopini *et al.*, 2011; Li and Jiang, 2011; Mancktelow, 2013). We addressed the loss of dimensionality information by resorting to X-ray micro computed tomography (X-ray microCT), a non-destructive technique used since 90s in different fields of geological sciences to image a rock sample in three dimensions (Denison and Carlson, 1997; Denison *et al.* 1997; Ketcham and Carlson, 2001).

MicroCT analyses were performed with a BIR Actis 130/150 Desktop Micro-focus CT/DR system at Dipartimento di Scienze dell'Ambiente e della Terra, Università degli Studi di Milano – Bicocca (see Zanchetta *et al.*, 2011 for method details). The samples were attached to a plastic sample holder with their maximum axis in a vertical position. The dimensions of the voxel (3D pixel, i.e. the resolution of the images) of the obtained images are x, y, z = 19 μm. The obtained 3D microCT image stacks were processed with the software Avizo™.

X-ray microCT produces stacks of 2D grey-scale value images (referred to as "slices") that allow observing the internal structure of a scanned object. As exhaustively reported in Denison *et al*. (1997), the contrast in an X-ray CT image is mainly caused by differences in X-ray absorption within the object due to variation in density and chemical composition. K-feldspar porphyroclasts and the matrix dominated by quartz appear generally lighter in color than biotite sheets (Fig. 4a, c, e), which define the main foliation. Mineral phases were identified by comparing grey-scale colored slices with grey values of the Back Scattered Electrons (BSE) images on thin section (Fig. 4): the comparison between SEM data (compositions and BSE images) and corresponding microCT slices allowed a reliable identification of mineral phases. As quartz and K-feldspar display grey values that are close to each other, it is difficult to apply a segmentation. In order to process the image automatically, we applied a threshold value to the main foliation to highlight wrapped porphyroclasts, making them appear dark on segmented images (Fig. 4b,d,f). The stable porphyroclasts method requires processing the slices representative of the XZ plane of the strain ellipsoid. Factors such as the isolation factor and the slipping effect (Passchier, 1987; Iacopini *et al*., 2011) were evaluated also on the XY and YZ planes (Fig. 4c-f).

The first and foremost consideration is that the use of microCT certainly increases the number of investigated clasts because hand samples are scanned. MicroCT minimizes the problems due to the isolation factor, as it becomes possible to only select the clasts that do not interact with each other. Moreover, observation in three dimensions allows a correct evaluation of the aspect ratios and radii of clasts, avoiding erroneous measurements that generate systematic errors in the vorticity evaluation (Iacopini *et al*., 2011).

X-ray microCT scanning was performed on the same two mylonitic orthogneisses from the Munsiari Thrust, on which we obtained the $^{40}Ar/^{39}Ar$ ages of the mylonitic foliation. Vaikrita Thrust rocks were not suitable for vorticity analysis. We analysed 152 and 32 porphyroclasts, ranging in size from 2.5 to 12 mm, from UT15-5 and UT15-6, respectively, to derive vorticity estimates (Fig. 5). The analysed sample volume was 130 cm^3 for UT15-5 and 10 cm^3 for UT15-6. We adopt the plot proposed by

Wallis *et al*. (1993) and the Rigid Grain Net (RGN) plot suggested by Jessup *et al*. (2007), considering all porphyroclasts as tailless. Vorticity numbers range between 0.53-0.58 (Fig. 5a) and 0.49-0.57 (Fig. 5b-c) for UT15-6 and UT15-5, respectively.

4. Discussion

In the frame of exhumation models proposed for the GHS, adding as much information as possible to the knowledge on the bounding shear zones of the GHS itself is a crucial task. Quantitative estimates of the flow kinematics have been increasingly used to deduce large scale tectonics from a variety of geodynamic settings (Iacopini *et al*., 2008; Xypolias, 2010; Xypolias *et al*., 2010 and references therein). The kinematic vorticity of major Himalayan tectonic discontinuities has been determined both for the STDS, especially in the Eastern Himalaya (Law *et al*., 2004, 2011; Jessup *et al*., 2006; Carosi *et al*., 2006, 2007) and for several sectors of the MCTz: NW India (Grasemann *et al*., 1999; Law *et al*., 2013), central Nepal (Larson and Godin, 2009; Larson *et al*., 2010), eastern Nepal (Jessup *et al*., 2006) and Bhutan (Long *et al*., 2011).

Our stable porphyroclasts analysis results (W_m = 0.49-0.58, Fig. 5) on two mylonitic orthogneisses from the Munsiari Thrust reveals a dominance of the pure shear component (65-60 %), which is higher than, but overlaps with, literature reports from the MCTz.

In the Sutlej valley (NW India), Grasemann *et al*. (1999) support a large pure shear component throughout the entire MCTz from ductile to late stage of ductile-brittle transition. They relate the shift from a simple shear dominated to a pure shear dominated flow to a decelerating strain path. In the same area, Law *et al*. (2013) combining stable porphyroclasts and quartz *c*-axis methods, obtained W_m = 0.75-0.82 (Sutlej valley) and 0.90-0.95 (Shimla klippe transect), suggesting a predominantly simple shear flow moving upward from the MCT towards the core of the GHS. In central Nepal, both Larson and Godin (2009) and Larson *et al*. (2010) obtain a large pure shear component (66-41 %) that decreases with structural distance from the MCTz (W_m = 0.50-0.68 to 0.78-0.87). In eastern

Nepal, Jessup *et al*. (2006) find W_m = 0.63-0.77, i.e. a pure shear component of 44 – 58 %. In Bhutan, Long *et al*. (2011) find a large component of pure shear.

The progressive rejuvenation of the structures toward the foreland (i.e. from Vaikrita to Munsiari Thrust) is supported by the age of shearing constrained along these structures. In the Bhagirathi valley, our results support an in sequence shearing from c. 8.17 to 4.8 Ma from Vaikrita to Munsiari Thrust. The same result has been obtained in the Alaknanda valley, where the age of the Vaikrita Thrust, 9 Ma (Montemagni *et al*., 2019) is older than that of the Munsiari Thrust, 5.4 Ma (this work). The age of both faults is similar but not identical in the two neighboring valleys, suggesting that movement in the MCTz was not rigorously cylindrical.

Our results (Fig. 6) support the model of *decelerating strain path* of Grasemann *et al*. (1999): at 9-8 Ma Vaikrita shearing records a higher vorticity, in agreement with Law *et al*. (2013), who analysed samples in the hangingwall of the MCT. At 5-4 Ma, well after the cessation of Vaikrita thrusting (Montemagni *et al*., 2019), the Munsiari Thrust becomes active. Our vorticity data together with published data support an increase of the pure shear component toward the base of the MCTz: we argue that the exhumation of the GHS is dominated by simple shear at deeper crustal level and, when deformation shifted toward shallower structural levels, simple shear decreases in favor of an increasing pure shear component. This shift in space of deformation regime is mirrored by a younging of mica ages.

5. Conclusions

1. The microCT, as already widely used in geological studies, is a useful tool to improve the estimate of kinematic vorticity using rigid porphyroclasts embedded in a matrix, thanks to its spatial resolution, the high number of investigated clasts and the possibility to inspect the third dimension.

2. In the Garhwal Himalaya, our results combined with already published data support an in-sequence shearing from c. 8 to c. 5 Ma from Vaikrita to Munsiari Thrust.

3. At the time the S2 foliation was formed, the Munsiari Thrust had a large pure shear component, compatible with a decelerating strain path.

Acknowledgements

We thank A. Risplendente (Università degli Studi di Milano) for his support during the electron microprobe analyses and V. Barberini (Università degli Studi di Milano Bicocca) for the assistance during $^{40}Ar/^{39}Ar$ dating. This research was financially supported by PRIN 2015EC9PJ5 (to C. Montomoli and R. Carosi) and by funds from Dipartimento di Scienze dell'Ambiente e della Terra, Università degli Studi di Milano Bicocca.

References

Arita, K., 1983. Origin of the inverted metamorphism of the lower Himalaya, central Nepal. *Tectonophysics*, **95**, 43-60.

Bosio, G., Malinverno, E., Villa, I.M., Di Celma, C., Gariboldi, K., Gioncada, A., Barberini, V., Urbina, M. and Bianucci, G., 2019. Tephrochronology and chronostratigraphy of the Miocene Chilcatay and Pisco formations (East Pisco Basin, Peru). *Newsl. Stratigr.*, doi: 10.1127/nos/2019/0525.

Burg, J.P., Brunel, M., Gapais, D., Chen, G.M. and Liu, G.H. 1984. Deformation of leucogranites of the crystalline Main Central Sheet in southern Tibet (China). *J. Struct. Geol*., **6**, 535–542.

Caby, R., Pecher, A. and Le Fort, P., 1983. Le grand chevauchement central himalayen: nouvelles donnees sur le metamorphisme inverse a' la base de la Dalle du Tibet. *Rev. Geol. Dynam. Geog. Phys*., **24**, 89–100.

Carosi, R., Montomoli, C. and Iaccarino, S., 2018. 20 years of geological mapping of the metamorphic core across Central and Eastern Himalayas. *Earth Sci. Rev.*, **177**, 124-138.

Carosi, R., Montomoli, C. and Visonà, D., 2007. A structural transect in the Lower Dolpo: Insights on the tectonic evolution of western Nepal. *J. Asian Earth Sci*., **29**, 407–423.

Carosi, R., Montomoli, C., Rubatto, D. and Visonà, D., 2006. Normal-sense shear zones in the core of the Higher Himalayan Crystallines (Bhutan Himalayas): evidence for extrusion? In: *Channel flow, ductile extrusion and exhumation in continental collision zones* (Law, R.D., Searle, M.P. and Godin, L., eds). *Geol. Soc. London Spec. Publ*., **268**, 425-444.

Carosi, R., Montomoli, C., Iaccarino, S., Massonne, H.-J., Rubatto, D., Langone, A., Gemignani, L. and D. Visonà, 2016. Middle to late Eocene exhumation of the Greater Himalayan Sequence in the Central Himalayas: Progressive accretion from the Indian plate, *Geol. Soc. Am. Bull.,* **128**, 1571-1592.

Denison, C. and Carlson, W.D., 1997. Three-dimensional quantitative textural analysis of metamorphic rocks using high-resolution computed X-ray tomography: Part II. Application to natural samples. *J. Metamorph. Geol*., **15**, 45-57.

Denison, C., Carlson, W.D. and Ketcham, R.A., 1997. Three-dimensional quantitative textural analysis of metamorphic rocks using high-resolution computed X-ray tomography. Part I: methods and techniques. *J. Metamorph. Geol*., **15**, 29–44.

Ferrill, D.A., Morris, A.P., Evans, M.A., Burkhard, M., Groshong Jr, R.H. and Onasch, C.M., 2004. Calcite twin morphology: a low-temperature deformation geothermometer. *J. Struct. Geol*., **26**, 1521-1529.

Fossen, H. and Cavalcante, G.C.G., 2017. Shear zones: a review. *Earth Sci. Rev.*, **171**, 434–455.

Godin, L., Grujic, D., Law, R.D. and Searle, M.P., 2006. Channel flow, ductile extrusion and exhumation in continental collision zones: an introduction. In: *Channel flow, ductile extrusion and exhumation in continental collision zones* (Law, R.D., Searle, M.P. and Godin, L., eds). *Geol. Soc. London Spec. Publ*., **268**, 1-23.

Grasemann, B., Fritz, H. and Vannay, J.-C., 1999. Quantitative kinematic flow analysis from the main central thrust zone (NW-Himalaya, India): implications for a decelerating strain path and the extrusion of orogenic wedges. *J. Struct. Geol.*, **21**, 837-853.

Heim, A.A. and Gansser, A., 1939. Central Himalaya: Geological Observations of the Swiss Expedition, 1936. *Hindustan Publishing, Delhi.*

Hodges, K., 2000. Tectonics of Himalaya and southern Tibet from two perspectives. *Geol. Soc. Am. Bull.*, **112**, 324–350.

Hodges, K.V., Parrish, R.R. and Searle, M.P., 1996. Tectonic evolution of the central Annapurna range, Nepalese Himalayas. *Tectonics*, **15**, 1264-1291.

Iacopini, D., Carosi, R., Montomoli, C. and Passchier, C.W., 2008. Strain analysis of flow in the Northern Sardinian Varisican Belt: recognition of a partitioned oblique deformation event. *Tectonophysics*, **221**, 345-359.

Iacopini, D., Frassi, C., Carosi, R. and Montomoli, C., 2011. Biases in three-dimensional vorticity analysis using porphyroclast system: limits and application to natural examples. *Geol. Soc. London Spec. Publ.*, **360**, 301-318.

Jain, A.K., Shreshtha, M., Seth, P., Kanyal, L., Carosi, R., Montomoli, C., Iaccarino, S. and Mukherjee P.K., 2014. The higher Himalayan Crystallines, Alaknanda – Dhauli Ganga Valleys, Garhwal Himalaya, India. In: *Geological Field Trips in the Himalaya, Karakoram and Tibet* (Montomoli, C., Carosi, R., Law, R., Singh, S. and Rai, S.M., eds). *J. Virtual Explorer Electronic Edition*, **47**, https://doi.org/10.3809/jvirtex.2014.00349.

Jessup, M.J., Law, R.D. and Frassi, C., 2007. The rigid grain net (RGN): an alternative method for estimating mean kinematic vorticity number (W_m). *J. Struct. Geol.*, **29**, 411-421.

Jessup, M.J., Law, R.D., Searle, M.P. and Hubbard, M.S., 2006. Structural evolution and vorticity of flow during extrusion and exhumation of the Greater Himalayan Slab, Mount Everest Massif, Tibet/Nepal: implications for orogen-scale flow partitioning. In: *Channel Flow, Extrusion, and Exhumation in Continental Collision Zones* (Law, R.D., Searle, M.P. and Godin, L., eds). *Geol. Soc. London Spec. Publ*., **268**, 379-414.

Ketcham, R.A. and Carlson, W.D., 2001. Acquisition, optimization and interpretation of X-ray computed tomographic imagery: applications to the geosciences. *Comput. Geosci.*, **27**, 381-400.

Larson, K.P. and Godin, L., 2009. Kinematics of the Greater Himalayan Sequence, Dhaulagiri Himal: implications for the structural framework of central Nepal. *J. Geol. Soc*., **166**, 25–43.

Larson, K.P., Godin, L. and Price, R.A., 2010. Relationship between displacement and distortion in orogens: linking the Himalayan foreland and hinterland in Central Nepal. *Geol. Soc. Am. Bull*., **122**, 1116-1134.

Law, R.D., Jessup, M.J., Searle, M.P., Francis, M., Waters, D. and Cottle, J.M., 2011. Telescoping of isotherms beneath the South Tibetan Detachment System, Mount Everest Massif. *J. Struct. Geol.*, **33**, 1569–1594.

Law, R.D., Searle, M.P. and Simpson, R.L., 2004. Strain, deformation temperatures and vorticity of flow at the top of the Greater Himalayan Slab, Everest Massif, Tibet. *J. Geol. Soc. Lond*., **161**, 305–320.

Law, R.D., Stahr, D.W., Francsis, M.K., Ashley, K.T., Grasemann, B. and Ahmad, T., 2013. Deformation temperatures and flow vorticities near the base of the Greater Himalayan Series, Sutlej Valley and Shimla Klippe, NW India. *J. Struct. Geol.*, **54**, 21–53.

Li, C. and Jiang, D., 2011. A critique of vorticity analysis using rigid clasts. *J. Struct. Geol.*, **33**, 203-219.

Long, S., McQuarrie, N., Tobgay, T. and Hawthorne, J., 2011. Quantifying internal strain and deformation temperature in the eastern Himalaya, Bhutan: Implications for the evolution of strain in thrust sheets. *J. Struct. Geol.*, **33**, 579-608.

Mancktelow, N.S., 2013. Behaviour of an isolated rimmed elliptical inclusion in 2D slow incompressible viscous flow. *J. Struct. Geol.*, **46**, 235-254.

Martin, A. J., 2017. A review of definitions of the Himalayan Main Central Thrust. International *J. Earth Sci*., **106**, 2131-2145.

Metcalfe, R.P., 1993. Pressure, temperature and time constraints on metamorphism across the Main Central Thrust zone and High Himalayan Slab in the Garhwal Himalaya. In: *Himalayan Tectonics* (Treloar, P.J. and Searle, M.P, eds). *Geol. Soc. London Spec. Publ*., **74**, 485–509.

Montemagni, C., Iaccarino, S., Montomoli, C., Carosi, R., Jain, A.K. and Villa, I.M., 2018. Age constraints on the deformation style of the South Tibetan Detachment System in Garhwal Himalaya. *It. J. Geosci*., **137**, 175-187.

Montemagni, C., Montomoli, C., Iaccarino, S., Carosi, R., Jain, A. K., Massonne, H. -J. and Villa, I. M., 2019. Dating protracted fault activities: microstructures, microchemistry and geochronology of the Vaikrita Thrust, Main Central Thrust zone, Garhwal Himalaya, NW India. *Geol. Soc. London Spec. Publ*., **481**, https://doi.org/10.1144/SP481.3.

Montomoli, C., Iaccarino, S., Carosi, R., Langone, A. and Visonà, D., 2013. Tectonometamorphic discontinuities within the Greater Himalayan Sequence in Western Nepal (Central Himalaya): nsights on the exhumation of crystalline rocks. *Tectonophysics*, **608**, 1349-1370.

Montomoli, C., Carosi, R. and Iaccarino, S., 2015. Tectonometamorphic discontinuities in the Greater Himalayan Sequence: a local or a regional feature? In: *Tectonics of the Himalaya* (Mukherjee S., van der Beek, P. and Mukherjee, P.K., eds). *Geol. Soc. London Spec. Publ.,* **412**, 21-41.

Passchier, C.W. and Trouw, R.A.J., 2005. *Microtectonics*. Berlin: Springer Verlag.

Passchier, C.W., 1987. Stable position of rigid objects in noncoaxial flow: a study in vorticity analysis. *J. Struct. Geol*., **9**, 679-690.

Robert, X., Van Der Beek, P., Braun, J., Perry, C. and Mugnier, J.L., 2011. Control of detachment geometry on lateral variations in exhumation rates in the Himalaya: Insights from low-temperature thermochronology and numerical modeling. *J. Geophys. Res. Solid Earth*, **116**(B5).

Searle, M.P., Law, R.D.,Godin, L., Larson, K.P., Streule, M.J., Cottle, J.M. and Jessup, M.J., 2008. Defining the Himalayan Main Central Thrust in Nepal. *J. Geol. Soc. London*, **165**, 523–534.

Searle, M.P., Metcalfe, R.P., Rex, A.J. and Norry, M.J., 1993. Field relations, petrogenesis and emplacement of the Bhagirathi leucogranite, Garhwal Himalaya. *Geol. Soc. London Spec. Publ.*, **74**, 429-444.

Singh, S., 2019. Protracted zircon growth in migmatites and in situ melt of Higher Himalayan Crystallines: U–Pb ages from Bhagirathi Valley, NW Himalaya, India. *Geosci. Front.*, **10**, 793-809.

Spencer, C.J., Harris, R.A. and Dorais, M.J., 2012. The metamorphism and exhumation of the Himalayan metamorphic core, eastern Garhwal region, India. *Tectonics*, **31**, 1–18.

Thakur, S.S., Patel, S.C. and Singh, A.K., 2015. A P–T pseudosection modelling approach to understand metamorphic evolution of the Main Central Thrust Zone in the Alaknanda valley, NW Himalaya. *Contrib. Mineral. Petrol.*, **170**, 1–26.

Valdiya, K.S. 1980. The two intracrustal boundary thrusts of the Himalaya. *Tectonophysics*, **66**, 323-348.

Wallis, S.R., Platt, J.P. and Knott, S.D., 1993. Recognition of syn-convergence extension in accretionary wedges with examples from the Calabrian arc and the eastern Alps. *Am. J. Sci.*, **293**, 463-495.

Weinberg, R.F., 2016. Himalayan leucogranites and migmatites: Nature, timing and duration of anataxis. *J. Metamorph. Geol.*, **34**, 821-843.

Whitney, D.L. and Evans, B.W., 2010. Abbreviations for names of rock-forming minerals. *Am. Mineral.*, **95**, 185-187.

Xypolias, P., 2010. Vorticity analysis in shear zones: a review of methods and applications. *J. Struct. Geol.*, **32**, 2072–2092.

Xypolias, P., Spanos, D., Chatzaras, V., Kokkalas, S. and Koukouvelas, I., 2010. Vorticity of flow in ductile thrust zones: examples from the Attico-Cycladic Massif (Internal Hellenides, Greece). In: *Continental Tectonics and Mountain Building: The Legacy of Peach and Horne* (Law, R.D., Butler, R.W.H., Holdsworth, R.E., Krabbendam, M. and Strachan, R.A., eds). *Geol. Soc. London Spec. Publ.*, **335**, 687-714.

Zanchetta, S., D'Adda, P., Zanchi, A., Barberini, V. and Villa, I.M., 2011. Cretaceous-Eocene compression in the central Southern Alps (N Italy) inferred from $^{40}Ar/^{39}Ar$ dating of pseudotachylytes along regional thrust faults. *J. Geodyn.*, **51**, 245-263.

Figure captions

Figure 1. (a) Simplified geological map of the Himalaya (modified after Weinberg, 2016). (b) The Bhagirathi area (after Searle *et al*., 1993 and Singh, 2019). The yellow stars show the structural position of the analyzed samples. (c) The Alaknanda – Dhauli Ganga area (from Montemagni *et al*., 2019). Position of analyzed sample is highlighted with a yellow star; samples from Montemagni *et al*., 2019 are shown with green stars.

Figure 2. Microstructures of selected samples. (a) K-feldspar porphyroclasts embedded by S2 biotite shows a top-to-the-SW shear sense (UT15-5); (b) quarter mats around K-feldspar porphyroclasts are coherent with a top-to-the-SW shear sense (UT15-5); (c) twinned feldspar porphyroclast wrapped by the S2 foliation, with asymmetric tails, show a top-to-the-SW shear sense (UT15-6); (d) group 4

biotite fish shows a top-to-the-SW shear sense (UT15-6); (e) muscovite forming the S2 schistosity in the calcschist of Munsiari Thrust; note bulging recrystallization in quartz (white arrow). Sigmoid aggregates show a top-to-SW shear sense (AK18-13); (f) type-I (white arrow) and II (black arrow) twinning in calcite (Ferrill *et al*., 2004; AK18-13); (g) garnet porphyroclast with inclusion-free rim. Note that garnet rim truncates the mylonitic S2 foliation (white arrow, Vaikrita Thrust, UT15-10); (h) late static muscovite crystals (white arrows; UT15-10). Mineral abbreviation after Whitney and Evans (2010).

Figure 3. $^{40}Ar/^{39}Ar$ age spectra and Ca/K vs age correlation diagrams. (a) and (b) Munsiari Thrust samples; (c) and (d) Vaikrita Thrust sample. In (b) and (d), range of Ca/K measured by EMP is highlighted by the grey inset.

Figure 4. MicroCT processed images of sample UT15-5. (a), (c) and (e) grey-scale images; (b), (d) and (f) threshold images. (a) and (b) 3D visualization of the sample; (c) and (d) visualization on the XY plane; (e) and (f) XZ plane. A scanned image of sample UT15-5 is also reported.

Figure 5. Results of the vorticity estimate using the (a), (b) RGN plot of Jessup *et al*. (2007) and (c) Wallis plot (Wallis *et al*., 1993). (c) The rose diagram outlying the main trend of the S2 foliation is also reported.

Figure 6. Schematic model for the study area. Our data and literature data suggest that deformation, at the base of the MCTz, is dominated by pure shear, which decreases moving structurally upward. (a) The shearing along the VT is recorded by micas on the main mylonitic foliation at 9-8 Ma.In that time span kinematic vorticity in the hangingwall of the VT is simple shear dominated (Law *et al*., 2013); (b) deformation shifted southwards: Vaikrita Thrust becomes inactive and static micas overgrow the main foliation at 7-6 Ma. Shearing along the MT is constrained by micas along the main

foliation at c. 5 Ma. Kinematic vorticity recorded at the base of the MCTz suggests a large pure shear component. Temporal bracket for the end of STDS shearing in the Alaknanda – Dhauli Ganga valleys from Montemagni *et al*. (2018). The simple and pure shear components of the general flow are qualitatively represented in the grey boxes.

STDS: South Tibetan Detachment System; VT: Vaikrita Thrust; MT: Munsiari Thrust; MCTz: Main Central Thrust zone; W_m: mean kinematic vorticity number. Mineral abbreviation as Whitney and Evans (2010).

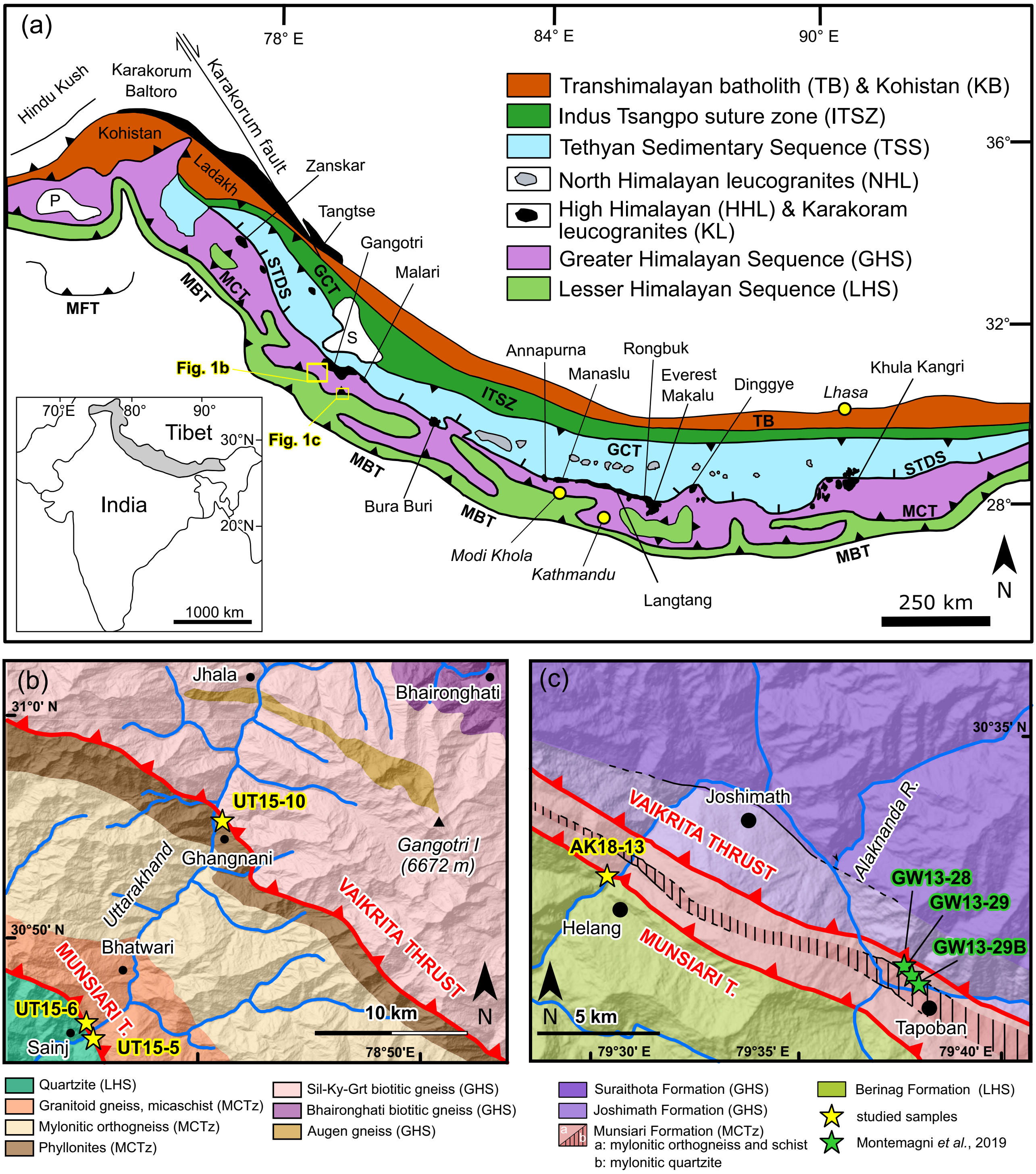
(a)
78° E
84° E
90° E
36°
32°
28°
Transhimalayan batholith (TB) & Kohistan (KB)
Indus Tsangpo suture zone (ITSZ)
Tethyan Sedimentary Sequence (TSS)
North Himalayan leucogranites (NHL)
High Himalayan (HHL) & Karakoram leucogranites (KL)
Greater Himalayan Sequence (GHS)
Lesser Himalayan Sequence (LHS)
Hindu Kush
Karakorum
Baltoro
Karakorum fault
Kohistan
Ladakh
Zanskar
Tangtse
Gangotri
Malari
P
S
MFT
MBT
MCT
STDS
GCT
ITSZ
TB
Fig. 1b
Fig. 1c
Annapurna
Rongbuk
Manaslu
Everest
Makalu
Dinggye
Lhasa
Khula Kangri
Bura Buri
Modi Khola
Kathmandu
Langtang
70°E
80°
90°
Tibet
30°N
India
20°N
1000 km
250 km
N
(b)
Jhala
Bhaironghati
31°0' N
UT15-10
Ghangnani
Uttarakhand
Gangotri I
(6672 m)
30°50' N
Bhatwari
MUNSIARI T.
VAIKRITA THRUST
UT15-6
Sainj
UT15-5
10 km
78°50'E
N
(c)
30°35' N
Joshimath
VAIKRITA THRUST
Alaknanda R.
AK18-13
Helang
MUNSIARI T.
GW13-28
GW13-29
GW13-29B
Tapoban
N
5 km
79°30' E
79°35' E
79°40' E
Quartzite (LHS)
Granitoid gneiss, micaschist (MCTz)
Mylonitic orthogneiss (MCTz)
Phyllonites (MCTz)
Sil-Ky-Grt biotitic gneiss (GHS)
Bhaironghati biotitic gneiss (GHS)
Augen gneiss (GHS)
Suraithota Formation (GHS)
Joshimath Formation (GHS)
Munsiari Formation (MCTz)
a: mylonitic orthogneiss and schist
b: mylonitic quartzite
Berinag Formation (LHS)
studied samples
Montemagni et al., 2019

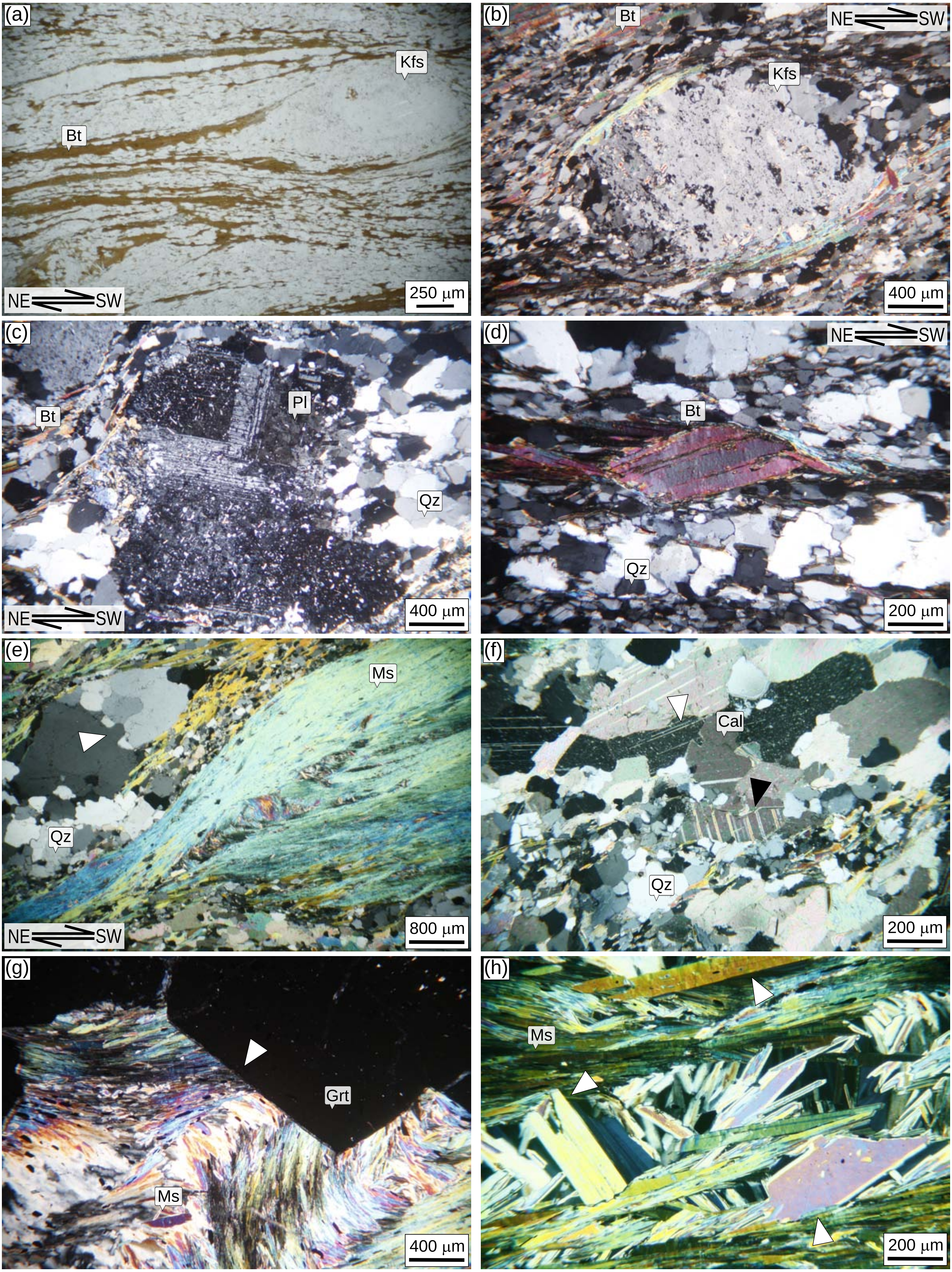
(a)
Kfs
Bt
NE SW
250 μm
(b)
Bt
NE SW
Kfs
400 μm
(c)
Bt
Pl
Qz
NE SW
400 μm
(d)
NE SW
Bt
Qz
200 μm
(e)
Ms
Qz
NE SW
800 μm
(f)
Cal
Qz
200 μm
(g)
Grt
Ms
400 μm
(h)
Ms
200 μm

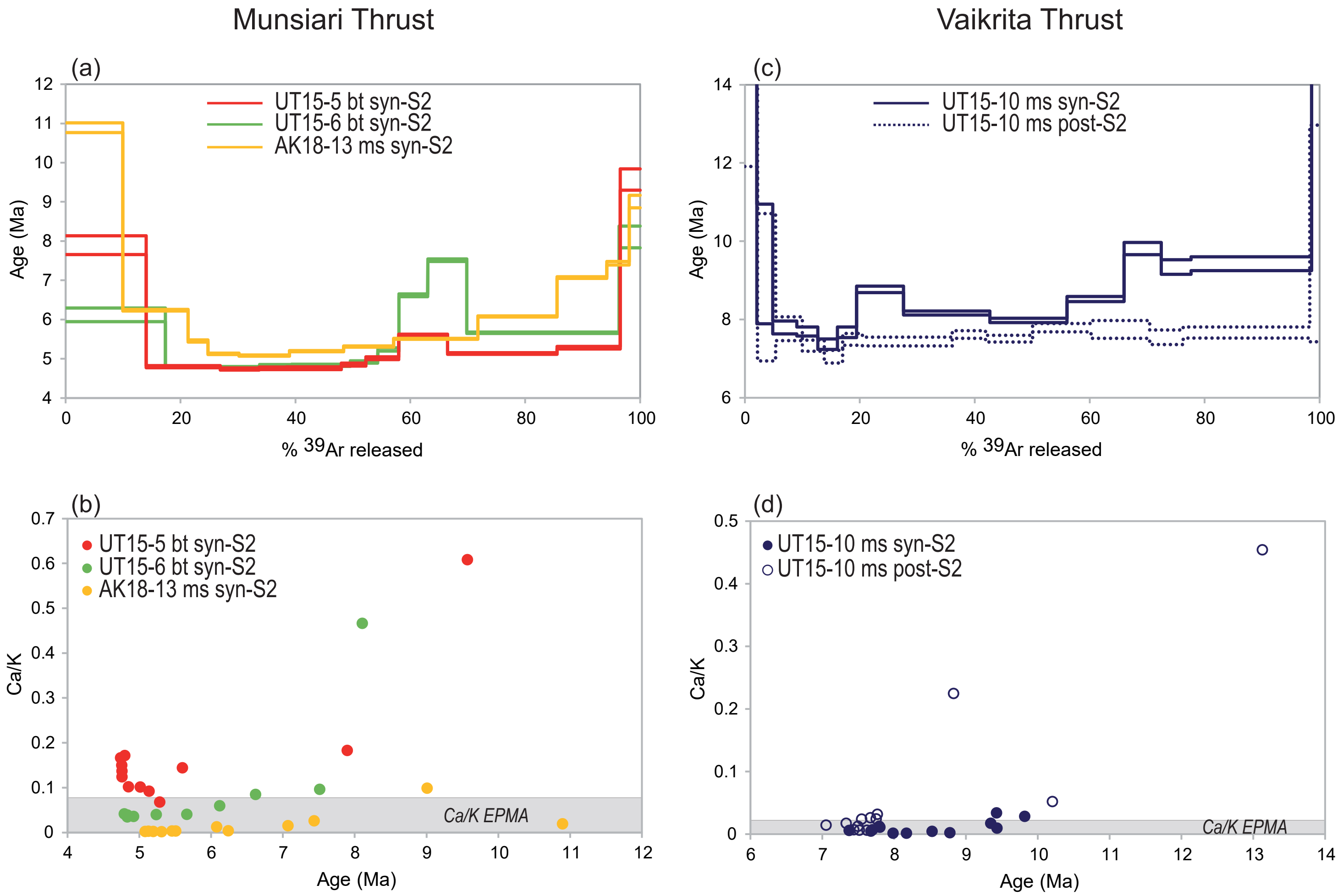
Munsiari Thrust
Vaikrita Thrust
(a)
UT15-5 bt syn-S2
UT15-6 bt syn-S2
AK18-13 ms syn-S2
Age (Ma)
% 39Ar released
(b)
UT15-5 bt syn-S2
UT15-6 bt syn-S2
AK18-13 ms syn-S2
Ca/K
Ca/K EPMA
Age (Ma)
(c)
UT15-10 ms syn-S2
UT15-10 ms post-S2
Age (Ma)
% 39Ar released
(d)
UT15-10 ms syn-S2
UT15-10 ms post-S2
Ca/K
Ca/K EPMA
Age (Ma)

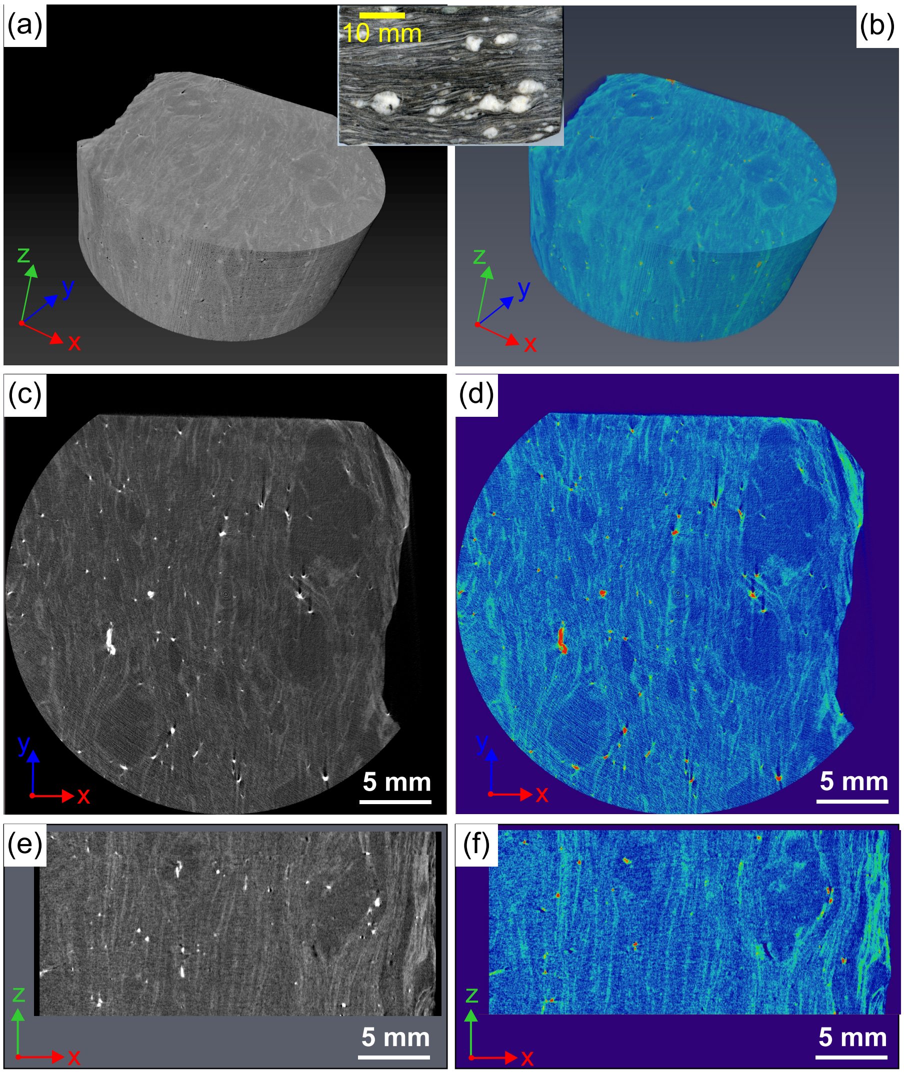
(a)
10 mm
(b)
(c)
(d)
(e)
(f)
5 mm
5 mm
5 mm
5 mm
z
y
x

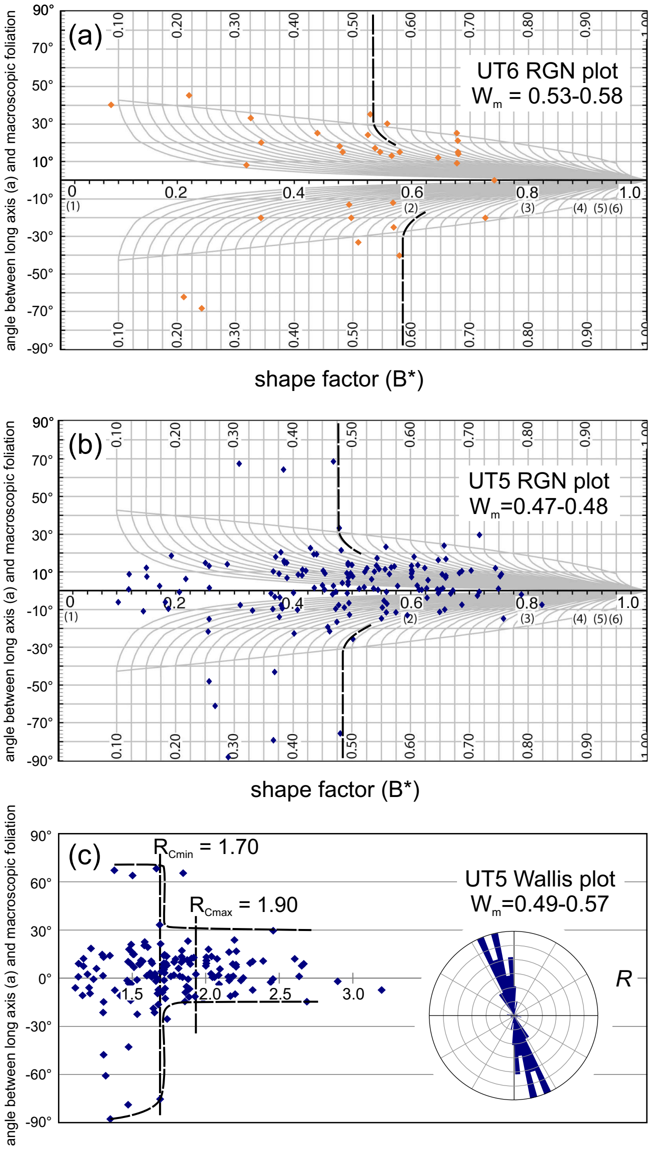
(a)
UT6 RGN plot
W$_m$ = 0.53-0.58
angle between long axis (a) and macroscopic foliation
shape factor (B*)
(b)
UT5 RGN plot
W$_m$=0.47-0.48
angle between long axis (a) and macroscopic foliation
shape factor (B*)
(c)
R$_{Cmin}$ = 1.70
R$_{Cmax}$ = 1.90
UT5 Wallis plot
W$_m$=0.49-0.57
R
angle between long axis (a) and macroscopic foliation

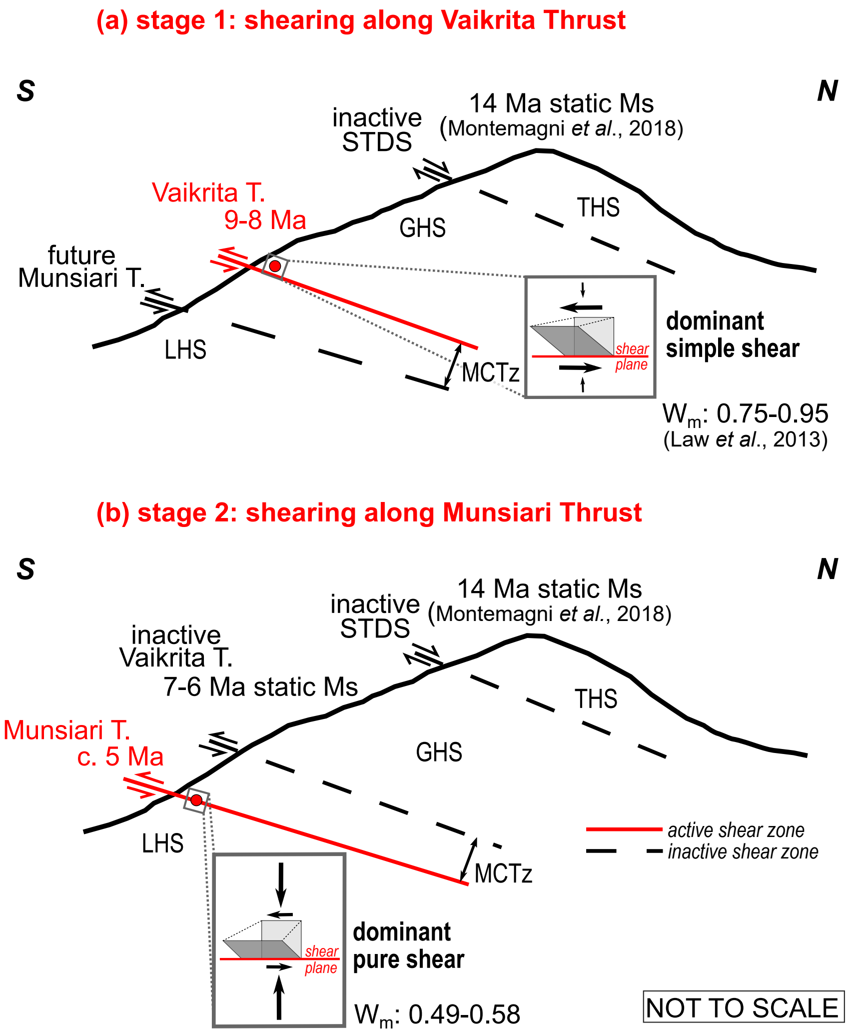
(a) stage 1: shearing along Vaikrita Thrust
S
N
inactive
STDS
14 Ma static Ms
(Montemagni et al., 2018)
Vaikrita T.
9-8 Ma
GHS
THS
future
Munsiari T.
LHS
MCTz
shear
plane
dominant
simple shear
W$_m$: 0.75-0.95
(Law et al., 2013)
(b) stage 2: shearing along Munsiari Thrust
S
N
inactive
STDS
14 Ma static Ms
(Montemagni et al., 2018)
inactive
Vaikrita T.
7-6 Ma static Ms
THS
Munsiari T.
c. 5 Ma
GHS
LHS
MCTz
active shear zone
inactive shear zone
shear
plane
dominant
pure shear
W$_m$: 0.49-0.58
NOT TO SCALE